Methods

Estimating photosynthetic capacity from leaf reflectance and Chl fluorescence by coupling radiative transfer to a model for photosynthesis

Nastassia Vilfan (iD)**, Christiaan van der Tol** (iD) **and Wouter Verhoef** (iD)

Wageningen University & Research Business unit Greenhouse Horticulture Droevendaalsesteeg 1, Wageningen, Netherlands

Summary

Author for correspondence:
Nastassia Vilfan
Tel: +31 317485104
Email: nastassia.rajhvilfan@wur.nl

- In photosynthesis models following the Farquhar formulation, the maximum carboxylation rate V_{cmax} is the key parameter. Remote-sensing indicators, such as reflectance ρ and Chl fluorescence (ChlF), have been proven as valuable estimators of photosynthetic capacity and can be used as a constraint to V_{cmax} estimation.
- We present a methodology to retrieve V_{cmax} from leaf ρ and ChlF by coupling a radiative transfer model, FLUSPECT, to a model for photosynthesis. We test its performance against a unique dataset, with combined leaf spectral, gas exchange and pulse-amplitude-modulated measurements.
- Our results show that the method can estimate the magnitude of V_{cmax} estimated from the far-red peak of ChlF and green ρ or transmittance τ, with values of root-mean-square error below 10 μmol CO_2 m^{-2} s^{-1}.
- At the leaf level, the method could be used for detection of plant stress and tested against more extensive datasets. With a similar scheme devised for the higher spatial scales, such models could provide a comprehensive method to estimate the actual photosynthetic capacity of vegetation.

Introduction

Monitoring photosynthesis through remote-sensed signals leads to a better understanding of vegetation canopies and their interaction with the environment. At least two optical indicators have been shown to respond to photosynthetic processes dynamically: Chl fluorescence (ChlF) and photochemical reflectance index (PRI). Both ChlF and PRI are intrinsically linked to photosynthesis, and have both been established as good estimators of leaf light use efficiency (LUE) and photosynthesis (for reviews, see Garbulsky *et al.*, 2011; Ač *et al.*, 2015). Developing methods for the estimation of photosynthesis from the two optical indicators is particularly relevant for the fast-developing field of precision agriculture (Tremblay *et al.*, 2011; Wieneke *et al.*, 2016), and for the European Space Agency's dedicated Fluorescence Explorer (FLEX) satellite mission (Drusch *et al.*, 2017).

In order to develop such methods, it is key to understand how the enzyme kinetics of photosynthesis are reflected in the dynamic changes of plant optical properties. The solar energy, absorbed by the leaf, undergoes one of three possible pathways: it can be used in photochemistry, emitted as ChlF, or dissipated as heat. This conversion of energy can be detected as a dynamic optical signature in the visible and near-infrared part of the leaf spectrum.

The light is captured by the light-harvesting antennae, and the energy is transferred to the photosynthetic reaction centres. From the captured light, *c.* 2% of light is directly emitted as ChlF. The spectrum of ChlF has a typical double peak, and ranges from *c.* 650 to 850 nm. The rest of the captured energy follows a complex process of photochemistry, eventually resulting in the fixation of CO_2.

However, in natural conditions, plants are often exposed to various stresses that lower their capacity to utilize the available light. Excess energy must then be effectively dissipated via one of the many photoprotective mechanisms of higher plants in order to prevent damage to the photosynthetic apparatus. For example, high light exposure causes rapid saturation of the photosynthetic reaction centres, and the fastest response of the photosynthetic membrane to excess light is to dissipate the surplus of energy as heat. This process is known as the nonphotochemical ChlF quenching (NPQ). It is closely related to the xanthophyll cycle, which involves an interconversion of three xanthophylls: violaxanthin via antheraxanthin into zeaxanthin, followed by a complex series of thylakoid conformational and pH changes, concluding with heat dissipation (Demmig-Adams & Adams, 1996; Ruban, 2016). These photoprotective mechanisms can be observed as dynamic changes in the green part of the visible spectrum, commonly expressed as the PRI (Gamon *et al.*, 1992).

In order to interpret the remotely sensed data, models are needed. Simple indices using only one or two spectral bands, such as PRI, may be insufficient due to the contributions of various leaf pigments and canopy structure to the few selected spectral bands (Gitelson *et al.*, 2017). Radiative transfer (RT) models can describe the light propagation within leaves and canopies based on biochemical and physical properties, enabling us to better decouple the contributions of individual parameters. Complementary to RT models, models for photosynthesis can explain the underlying biochemical processes. Coupling the two types of models would provide a unique insight into the connection between optical and biochemical properties of vegetation.

State-of-the-art models, such as the Soil–Canopy Observation of Photosynthesis and Energy balance (SCOPE) model (Van der Tol *et al.*, 2009), are able to quantify both the variability of photosynthesis and spectral changes at different temporal and spatial scales by employing the biochemical and RT properties of vegetation.

At the leaf level, SCOPE employs two models: a biochemical model, able to explain the relationship between ChlF, photosynthesis and NPQ under different environmental conditions (Van der Tol *et al.*, 2014); and an RT model, FLUSPECT (Vilfan *et al.*, 2016). Both of the models are well tested, computationally affordable, and can function separately, providing independent outputs.

The biochemical model follows Farquhar's 1980s photosynthesis formulation (Farquhar *et al.*, 1980), in which the maximum carboxylation rate V_{cmax} of leaves is a key parameter. V_{cmax} determines the maximum photosynthesis rate of a plant under optimal conditions, and it has a great influence on the modelled photosynthesis.

FLUSPECT simulates leaf reflectance ρ, transmittance τ, and ChlF spectra as a function of leaf pigment content and structure. Recently, FLUSPECT has been extended to simulate the dynamics of green ρ as a function of the xanthophyll de-epoxidation, an RT analogy to the PRI (Vilfan *et al.*, 2018).

In this study, we couple the two leaf models via ChlF and photochemical ρ parameters, and effectively link spectral to biochemical properties. Attempts to create such links have been made before; however, in most cases, PRI and ChlF as proxies of photosynthesis were studied separately (for a review, see Grace *et al.*, 2007), with a few exceptions (Cheng *et al.*, 2013; Atherton *et al.*, 2016). The link of ρ dynamics to photochemistry is generally addressed with the use of the PRI, and relations of spectral information to photosynthetic parameters have mostly been defined via regression models (Cheng *et al.*, 2013; Serbin *et al.*, 2015; Zhang *et al.*, 2016; Dechant *et al.*, 2017; Liu *et al.*, 2017). With the introduction of dynamic xanthophyll ρ into FLUSPECT, we could avoid the use of PRI and approach changes in both ρ and ChlF in an RT-based manner. We developed a scheme that links leaf V_{cmax} to ρ, τ and ChlF. Such a model has not been published before.

The coupled model enabled us to devise a method for the retrieval of the V_{cmax} from hyperspectral measurements of leaf ChlF and ρ or τ. In this study, we describe the coupled model

and the retrieval method. We test its performance against a unique dataset, with combined leaf spectral, gas exchange and pulse-amplitude-modulated (PAM) measurements. We evaluate the sensitivity of the method to ChlF and ρ, and we discuss whether combined they provide an even better constraint to the retrieval of leaf photosynthetic parameters.

Materials and Methods

Laboratory experiment

The experiment was conducted in the laboratories of Forschungszentrum Jülich in February and March 2014. Sugar beet (*Beta vulgaris* L.) and barley (*Hordeum vulgare* L.) plants were grown in pots under controlled conditions in a glasshouse in Forschungszentrum Jülich between December 2013 and March 2014. Owing to the limited winter light conditions, the natural light was complemented with artificial light from growth lamps for $15 \, h \, d^{-1}$. The plants used in this experiment were grown under a light intensity of *c.* $1000 \, \mu mol \, m^{-2} \, s^{-1}$ (measured with a quantum sensor, LI-190SL; Li-Cor Inc., Lincoln, NE, USA). When the plants were fully grown, some of the pots grown under full light were exposed to water deficits. For a full description of growth conditions, see Vilfan *et al.* (2016). Measurements were collected on the same leaves in two separate experimental settings.

The first set-up, 'Chamber dataset', is presented in Fig. 1. It consisted of a portable gas-exchange system (LI-6400; Li-Cor Inc.) connected to a (1) clear top MiniPAM Adapter (6400-10; Li-Cor Inc.) housing the pulse-amplitude-modulated fluorescence system (Mini-PAM-II; Heinz Walz GmbH, Effeltrich, Germany); and (2) a spectroradiometer (FieldSpec 4; Analytical Spectral Devices, Boulder, CO, USA; 350–2500 nm, 3 nm visible and near-infrared spectral resolution). The gas-exchange chamber bottom was equipped with an airtight slot, fitting an optical fibre of the spectroradiometer. The top could not be adjusted to house the optical fibre due to technical limitations. The chamber was illuminated externally with a cold halogen lamp (KL 2500 LCD; Schott Benelux BV, Culemborg, Netherlands). The lamp was positioned to illuminate the chamber under an angle of *c.* 15°, ensuring that the whole leaf surface within the chamber was illuminated and not shaded by the PAM optical fibre. A short-pass filter can be slotted into the opening of the lamp, which cuts off the incoming light spectrum above *c.* 700 nm. This allowed for measurements of forward ChlF signal ('forward' referring to the emission being in same direction as the excitation radiation, which means in our set-up the ChlF emanating from the abaxial side of the leaf turned away from the light source above the leaf) from *c.* 700 to 850 nm. With this set-up, almost simultaneous measurements of passive and active ChlF, τ, and gas-exchange measurements were taken under controlled conditions.

Measurements were taken on attached leaves of intact plants using one or two healthy and fully developed leaves per pot. The leaf was positioned in the chamber with its adaxial side facing the light source. The gas-exchange system was set to a constant leaf temperature of 25°C, constant air humidity, and a CO_2 concentration of 400 ppm. We measured both light and CO_2 curves for
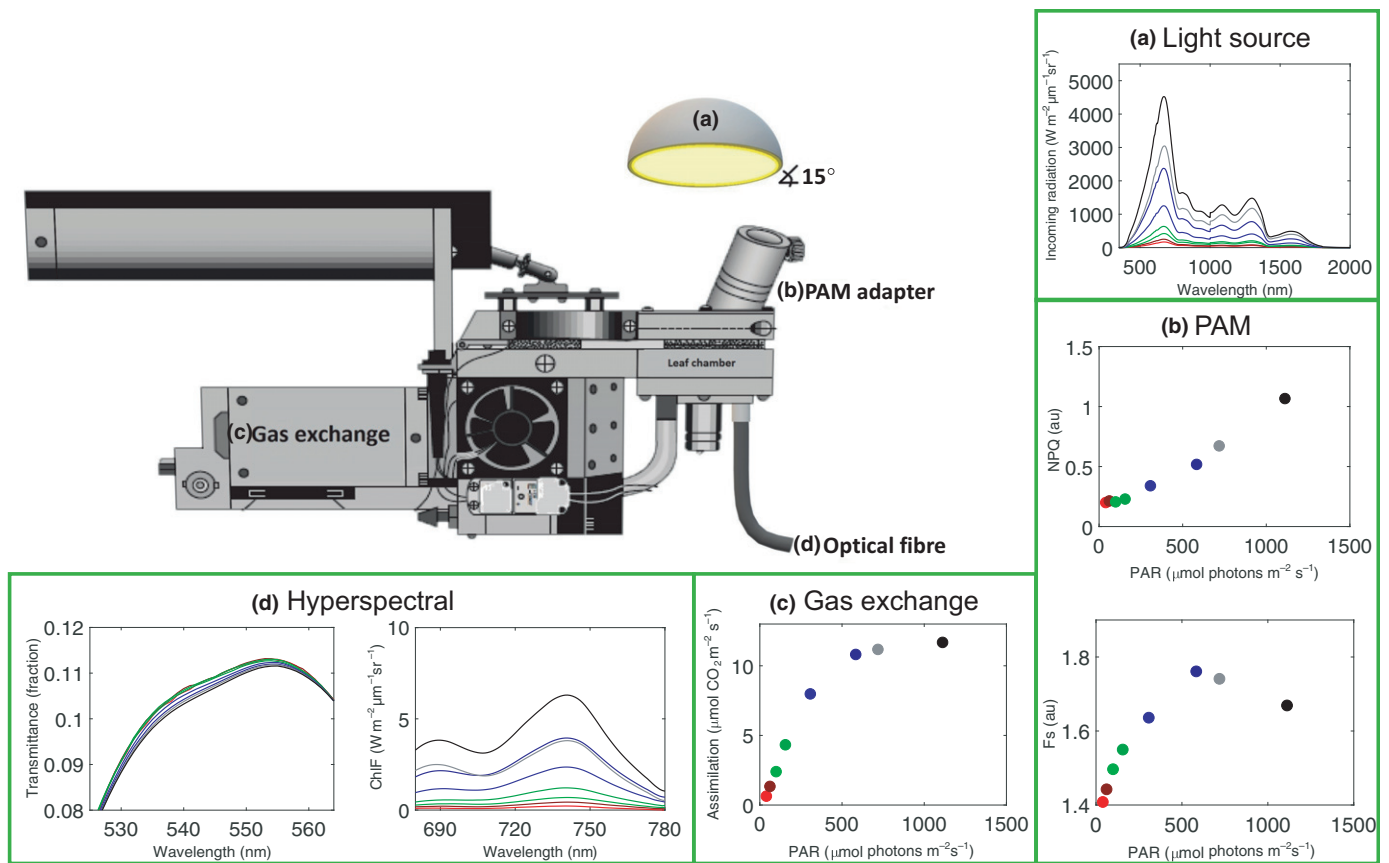
Fig. 1 A schematic representation of the 'chamber dataset' measurement set-up for a representative case of light-response curves of a barley leaf. Samples were illuminated with a cold blue light source (a). The following measurements were taken: (b) pulse amplitude modulation (PAM) fluorometry (nonphotochemical quenching (NPQ), steady state fluorescence F_s, and photochemically active radiation (PAR) are shown); (c) gas exchange (assimilation rate); and (d) spectral measurements (Chl fluorescence and transmittance). A red cut-off filter was slotted between the light source and the sample (not shown). Gas-exchange image used and modified by permission of Li-Cor Biosciences.

each leaf. Per each leaf, the light curve was measured first, directly followed by the measurement of the CO_2 curve, under illumination of $1000\,\mu mol\,m^{-2}\,s^{-1}$. The measured leaf surface and the position of the set-up were kept constant. Light intensities and CO_2 concentrations were adjusted manually in the following sequences of approximately:

1 0, 50, 100, 150, 250, 350, 500, 700, 1000, $1300\,\mu mol\,m^{-2}\,s^{-1}$,

2 400, 50, 100, 150, 250, 350, 500, 700, 900, 1200, 700, 400 ppm CO_2.

Each measurement consisted of the following sequence of recordings: gas exchange, followed by the transmitted radiance recorded with the spectroradiometer, the filtered transmitted radiance recorded with the spectroradiometer after slotting the filter into the opening of the lamp, and the active PAM measurement at the top of the leaf after removing the filter. The procedure was repeated for each change of either illumination or CO_2 conditions. Before each recording, we waited for the gas-exchange conditions to stabilize, 5 min on average, and up to 20 min for a change in the illumination conditions.

A standard reflectance panel (Spectralon; Labsphere, North Sutton, NH, USA) was used separately to estimate the incident and the filtered incident radiation of the lamp and the exact transmittance of the filter for each light intensity. The panel was positioned at the same distance from the light source as the leaf.

Each radiance measurement was the average of five individual measurements over the region of 350–2500 nm, using a 136 ms integration time. Transmittance and forward ChlF spectra were calculated using the standard formulas as described in Vilfan *et al.* (2016). It should be noted that the measurements of filtered radiance below 700 nm (and consequentially the red peak of ChlF) are unreliable due to the cut-off filter's characteristics. Moreover, the relative positioning of the reflectance panel, as well as the shape and characteristics of the gas-exchange chamber, might have contributed to additional scattering and inaccuracies in the calculated ChlF spectra. Furthermore, many hyperspectral measurements of barley had to be excluded from the study because the leaves were too small to cover the surface of the entire leaf chamber, contaminating the measurements with additional illumination.

LUE was calculated from gas-exchange data as:

$$LUE = \frac{A}{iPAR} \qquad \text{Eqn 1}$$

where A ($\mu mol\,CO_2\,m^{-2}\,s^{-1}$) is the assimilation rate and iPAR the incoming photosynthetically active radiation (PAR;

μmol m^{-2} s^{-1}) (Peñuelas *et al.*, 1995; Barton & North, 2001; Gitelson *et al.*, 2015).

From τ, we calculated the PRI as $(R_{531} - R_{570})/(R_{531} + R_{570})$. For a better comparison of the spectral measurements of different leaves, we normalized both the PRI and ChlF at the far-red peak (F_{740}) to their respective unstressed reference values (PRI′ and F'_{740}). By subtracting PRI′ from all values of PRI and F'_{740} from F_{740}, we obtained ΔPRI and ΔF_{740}, respectively. For the light responses, PRI′ and F'_{740}) were obtained from the spectrum measured at the lowest illumination (50 μmol m^{-2} s^{-1}), and for CO$_2$ curves from the spectrum measured at 1200 ppm CO$_2$.

For PAM measurements, standard procedures were followed (instruction manual for MINI-PAM-II; Maxwell & Johnson, 2000). During each measurement, a short, intense pulse of light was given, from which the quantum yield of photosystem II (PS-II) Φ$_{PSII}$ and electron transport rate (ETR) were calculated. ETR is automatically calculated by the accompanying software of the instrument, assuming an absorption coefficient of 0.84. Φ$_{PSII}$ reflects the proportion of light absorbed by PS-II that is used for photochemistry and was calculated as:

$$\Phi_{PSII} = \frac{F'_m - F_s}{F'_m} \qquad \text{Eqn 2}$$

where F_s is the steady state ChlF and F'_m is light-adapted maximum ChlF yield.

In the early morning, before the start of the measurement setup, PAM measurements were taken on dark-adapted leaves. This allowed for the calculation of minimal and maximal dark-adapted ChlF, F_o and F_m, respectively, and subsequently the NPQ:

$$NPQ = \frac{F_m - F'_m}{F'_m}, \qquad \text{Eqn 3}$$

where F_m represents the maximal dark-adapted ChlF yield. Because the information of PAM experiments is contained in the ratios, we normalized the signals to F_o. Since ETR, Φ$_{PSII}$ and NPQ are also outputs of the photosynthesis model, these measurements provided important additional insights into the model.

The second set-up, the 'FluoWat dataset', is described in detail in Vilfan *et al.* (2016). Measurements of bidirectional leaf ρ, τ, and ChlF were collected with the FluoWat leaf-clip, coupled to the same spectroradiometer that was used in the first set-up. The leaf clip has two openings for the fibre optics and one light entrance, fitting both a light source at a 45° angle and a short-pass filter (< 650 nm, TechSpec; Edmund Optics GmbH, Mainz, Germany). For more details on the FluoWat leaf clip design, see Van Wittenberghe *et al.* (2013). The samples were illuminated with the same cold light lamp as in the first set-up. We used measurements taken under three different light intensities, with iPAR of *c.* 200, 500 and 700–800 μmol m^{-2} s^{-1}.

Leaf models in SCOPE

FLUSPECT FLUSPECT is an RT model for the leaf, based on the model PROSPECT (Jacquemoud & Baret, 1990), where the

absorption is a function of the concentrations and specific absorption coefficients (SACs) of pigments and water. FLUSPECT computes ρ and τ spectra from 400 to 2500 nm, as well as ChlF spectra from 640 to 850 nm. It is implemented in MATLAB and published under GNU General Public License at https://github.com/christiaanvandertol. Input parameters, together with their definitions and standard values, are provided in Table 1. For a published full description of the model (FLUS-PECT-B), see Vilfan *et al.* (2016).

In this study, we use the latest version of FLUSPECT, called FLUSPECT-CX (Vilfan *et al.*, 2018), which is able to simulate changes in green ρ from *c.* 500 to 570 nm, as a function of the xanthophyll de-epoxidation parameter C_x, an RT analogy to the PRI. Moreover, in FLUSPECT-CX we adopted the SAC for antho-cyanins as well as recalibrated SACs for chlorophylls and carotenoids from PROSPECT-D (Féret *et al.*, 2017).

Changes in ChlF spectra can be simulated by varying η$_I$ and η$_{II}$: the fluorescence quantum efficiency parameters for PS-I and PS-II, respectively. In analogy to SACs, FLUSPECT uses two spectra for the probability density function φ to describe the spectral distribution of emitted ChlF: φ$_I$ and φ$_{II}$, one for each of the PS-I and PS-II. The two functions were adopted from Franck *et al.* (2002) and can be linearly mixed. However, owing to systematic discrepancies between measured and simulated ChlF spectra, φ has recently been recalibrated into a single spectrum for φ, with a single fluorescence quantum efficiency parameter η (C. Van der Tol *et al.*, unpublished), used in this study.

FLUSPECT can be inverted and its parameters estimated from measured spectra. However, FLUSPECT cannot explain the underlying processes of photosynthesis related to the dynamic parameters, such as C_x and η. They can, however, be estimated indirectly with the biochemical model that describes the relationship between ChlF, photosynthesis, and NPQ.

The biochemical model The biochemical model used in SCOPE simulates the photosynthetic rate and fluorescence quantities as measured with PAM, as a function of absorbed light, leaf temperature, relative humidity and the concentrations of CO$_2$ and oxygen (O$_2$). It follows Farquhar's formulation (Farquhar *et al.*, 1980), where the assimilation of CO$_2$ depends on electron transport and carboxylation, and the actual rate of assimilation is determined by the most limiting of these processes. Maximum carboxylation rate per leaf area under light-saturated conditions V_{cmax} is the key parameter in this model. Input parameters of the biochemical model are provided in Table 1. Only parameters relevant for this study are shown.

We used the empirical relationship between photochemical and fluorescence yield for unstressed conditions described in Van der Tol *et al.* (2014), a nonlinear relationship between the relative light saturation of photosynthesis and nonradiative energy dissipation in plants of different species calibrated to active ChlF measurements. To calculate the probability of the different fates of the excitation energy, it uses rate coefficients K: K_p and K_n for the photochemical ChlF quenching (PQ) and NPQ, respectively, and K_d and K_f for heat dissipation and fluorescence, respectively.

Table 1 List of parameters for the SCOPE leaf models.

Parameter	Interpretation	Range	Standard value	Unit	Origin
Leaf optical: FLUSPECT					
C_{ab}	Chlorophyll $a + b$ content	0–100	40	$\mu g\,cm^{-2}$	PROSPECT-D
C_{car}	Total carotenoid content	0–30	10	$\mu g\,cm^{-2}$	PROSPECT-D
C_{ant}	Anthocyanin content	0–10	0	$\mu g\,cm^{-2}$	PROSPECT-D
C_w	Water content	0–0.4	0.009	cm	PROSPECT
C_{dm}	Dry matter content	0–0.5	0.012	$g\,cm^{-2}$	PROSPECT
N	Leaf mesophyll structure parameter	1–4	1.4	—	PROSPECT
C_s	Senescence material (brown pigments)	0–0.6	0	arbitrary units	PROSPECT
η	Fluorescence quantum efficiency	0–0.2	0.01	—	FLUSPECT
C_x	Photochemical reflectance parameter	0–1.5	0	—	FLUSPECT
Leaf physiology: biochemical					
V_{cmax}	Maximum carboxylation capacity	0–250	70	$\mu mol\,CO_2\,m^{-2}\,s^{-1}$	
m	Ball–Berry stomatal conductance param.	2–20	8	—	
Rd_{param}	Parameter for dark respiration	0.001–0.03	0.015	—	
K_o^n	Fitting parameter for K_n (Eqn 4)	2–6	2.48	—	
β	Fitting parameter for K_n (Eqn 4)	0–10	0.114	—	
γ	Fitting parameter for K_n (Eqn 4)	0–10	2.83	—	

Two outputs are particularly relevant for this study: the fluorescence emission efficiency ε, expressed as the ratio of the steady state F_s to the dark-adapted fluorescence yield F_o; and K_n, which is considered to be equivalent to NPQ, and is calculated as follows:

$$K_n = \frac{K_n^0(1 + \beta)x^\gamma}{\beta + x^\gamma} \qquad \text{Eqn 4}$$

where K_n^0, γ and β are fitting parameters, and x is a measure for the light saturation of photosynthesis, calculated as:

$$x = 1 - \frac{\phi_p}{\phi_p^o}. \qquad \text{Eqn 5}$$

ϕ_p and ϕ_p^o represent the photochemical yield and the photochemical yield of dark-adapted state, respectively.

Dark-adapted fluorescence yield is then computed as:

$$F_o = \frac{K_f}{K_f + K_p + K_d} \qquad \text{Eqn 6}$$

and the steady state fluorescence as:

$$F_s = F_m'(1 - \phi_p). \qquad \text{Eqn 7}$$

Here, it should be noted that F_s, and consequently ε, are related to K_n through the calculation of F_m':

$$F_m' = \frac{K_f}{K_f + K_d + K_n} \qquad \text{Eqn 8}$$

Coupling the leaf models

FLUSPECT and the biochemical model have parameters related to photosynthesis in common, and this makes it possible to retrieve photosynthesis from the measured spectra of ChlF and τ. The two dynamic input parameters of FLUSPECT, η (the emission efficiency of fluorescence) and C_x (the absorption SAC for the xanthophyll cycle dynamics) are related to the outputs ε (F_s/F_o) and K_n (the rate coefficient for NPQ) of the biochemical model, and the simplest possible relation is a linear one.

To couple C_x to K_n, we adopt the relation of Vilfan *et al.* (2018):

$$C_x = 0.3187 \times \text{NPQ} \qquad \text{Eqn 9}$$

Similarly, η and ε are coupled as:

$$\eta = \varepsilon \times \varsigma \qquad \text{Eqn 10}$$

where ς is a scaling factor, calculated as a ratio of a typical value of η to a typical value of ε, with a value of 0.007, which represents the quantum efficiency of fluorescence in a dark-adapted leaf. This scaling is necessary because $\varepsilon = F_s/F_o$ is a relative value, whereas η is an absolute emission efficiency.

Retrieving maximum carboxylation capacity

V_{cmax} was retrieved in three ways, notably using gas exchange (method 1), PAM data (method 2), and hyperspectral measurements (method 3). Each method was applied to both the CO_2 and the light response curves, resulting in six sets of values for V_{cmax}. Method 1 (gas exchange) is the traditional way of retrieving V_{cmax}; therefore, we used the values retrieved with this method to validate the other two methods. Fig. 2 provides an overview of these methods, Table 1 default parameters of the biochemical model, and Table 2 presents the retrieved parameters, their boundaries and constraints.

For method 1, we retrieved V_{cmax} by inverting the biochemical model only, by minimizing the squared difference between measured and simulated assimilation rates A, following Kosugi & Matsuo (2006), Walker *et al.* (2014), and Zheng *et al.* (2017).

Measured values of PAR, leaf temperature, CO_2 and water vapour were used to force the model.

In method 2, we minimized the quadratic difference between modelled and (PAM) measured F_s and NPQ (Fig. 2a). In order to achieve an accurate fit of measured vs modelled F_s and NPQ, we fitted not only V_{cmax} but also the three empirical parameters of Van der Tol *et al.* (2014) for NPQ, notably K_n^0, γ and β (Eqn 4). With this method we could test the potential of using steady-state ChlF and NPQ data to retrieve photosynthesis from the biochemical model, in the absence of the informative measurements with the saturating flashes F_m and F_m').

In method 3, we used only the spectroscopy measurements to retrieve V_{cmax}, which was our ultimate aim (Fig. 2b). This method enabled us to test whether V_{cmax} in the combined radiative transfer and biochemical model can be sufficiently constrained by passive ChlF and τ data. A narrow band of ChlF at the far-red peak (730–750 nm) and of green τ (525–545 nm) were selected as the constraint for the model inversion. We retrieved V_{cmax} and the additional parameters K_n^0 and ς (Table 2) by minimizing the squared difference between the simulated and measured spectra (Eqn 11) for the whole-light- or CO_2-response curve at once. In this retrieval, the other parameters of FLUSPECT, notably the pigments and leaf structure parameter N, were kept to leaf-specific values. These values were retrieved once per leaf before the retrieval of V_{cmax}, K_n^0 and ς, and were assumed not to change during the light- and CO_2-response curves (Table 1). In this way, we attributed the dynamic changes to the τ spectrum to the xanthophyll cycle, and thus to C_x and K_n (Eqns 9, 10).

In all three methods, a trust-region algorithm was applied in MATLAB using the built-in function lsqnonlin to minimize a cost function:

$$C = (M - S)^2 \qquad \text{Eqn 11}$$

where M is the measured data and S the corresponding simulation (for the three methods: gas exchange, PAM data, and hyperspectral data). For method 3, M and S were matrices of multiple spectra: one spectrum for each of the 10 points on the CO_2-response curve or the eight points on the light-response curve. These spectra included τ and forward ChlF. Because method 3 only uses spectra as input (and no gas-exchange or PAM data), it was also applied to the additional FluoWat leaf clip dataset. The advantage of the FluoWat leaf clip data is that it provided not only the forward measurements (transmittance τ and ChlF at the shaded side), but also the backward measurements (reflectance ρ and ChlF at the illuminated side). However, due to some nonisotropic scattering and specular reflectance present in the ρ of some samples, we had to normalize the spectra of each light curve by subtracting the ρ at 565 nm. At this wavelength, the xanthophyll cycle ceases to have an effect on the spectra simulated by the FLUSPECT model.

We fitted ρ and backward ChlF, τ and forward ChlF, and both ρ and τ and forward and backward ChlF together to test the dependence of the performance on the side of the leaf that is measured.

Evaluating the model inversion

For method 1, we compared the V_{cmax} retrieved from the light-response curve with those retrieved with the CO_2-response curves. These retrievals were then used to validate the other methods. We evaluated the goodness-of-fit of V_{cmax}, A, and other variables by calculating the root-mean-squared error (RMSE) and Pearson's correlation coefficient R^2. The number of data points is slightly different among the three methods due to unrealistic values caused by occasional human error in the measurements, such as light pollution, vibrations during measurements, or incorrect measurement light and pulse settings of the PAM system.

The retrieval accuracy was evaluated for the chamber dataset with the relative RMSE. We further investigated the sensitivity of τ and ChlF spectra to the relevant parameters, the sensitivity of the retrievals to the starting values of the trust-region algorithm, and the ill-posedness of the retrieval. We calculated the Jacobian matrices J for τ and ChlF of the model for one representative sample. To obtain comparable values of the sensitivities and to normalize J, we multiplied J by the span of each parameter (see Table 2).

Error propagation in the retrieved parameters due to the measurement noise was estimated as:

$$E(\Delta p \Delta p^{\mathrm{T}}) = (J^{\mathrm{T}} J)^{-1} \sigma_r^2 \qquad \text{Eqn 12}$$

where the standard deviations of the retrieved parameters σ_p are found as the square roots of the diagonal elements of this matrix. σ_r is the SD of the measurements due to the measurement noise. For a full derivation of Eqn 12, refer to Vilfan *et al.* (2018).

Results

Optical and physiological measurements

In Fig. 3 we display different physiological and optical responses of leaves to variations in CO_2 concentrations and illumination. Assimilation increases with both increasing CO_2 and illumination intensity, until a plateau is reached. The initial slope of the assimilation curve represents the maximum LUE of the leaf, whereas the plateau signifies the light-saturated rate of photosynthesis (Björkman, 1981).

For the case of CO_2 curves, the indicators of photosynthetic capacity (A, LUE and Φ_{PSII}) continuously increase until the external concentration of *c.* 700 ppm CO_2, when the maximum assimilation and efficiency are reached. NPQ and PRI respond similarly, with the highest response at the lowest CO_2 concentrations. The ChlF response, however, is negligible. For the case of light-response curves, assimilation and ChlF increase with increasing light, whereas LUE, ΔPRI and Φ_{PSII} decrease.

When comparing measured spectral responses of ΔPRI and ΔF_{740} to physiological variables (Fig. 4), it is immediately evident that the two types of leaf response curves do not generate the
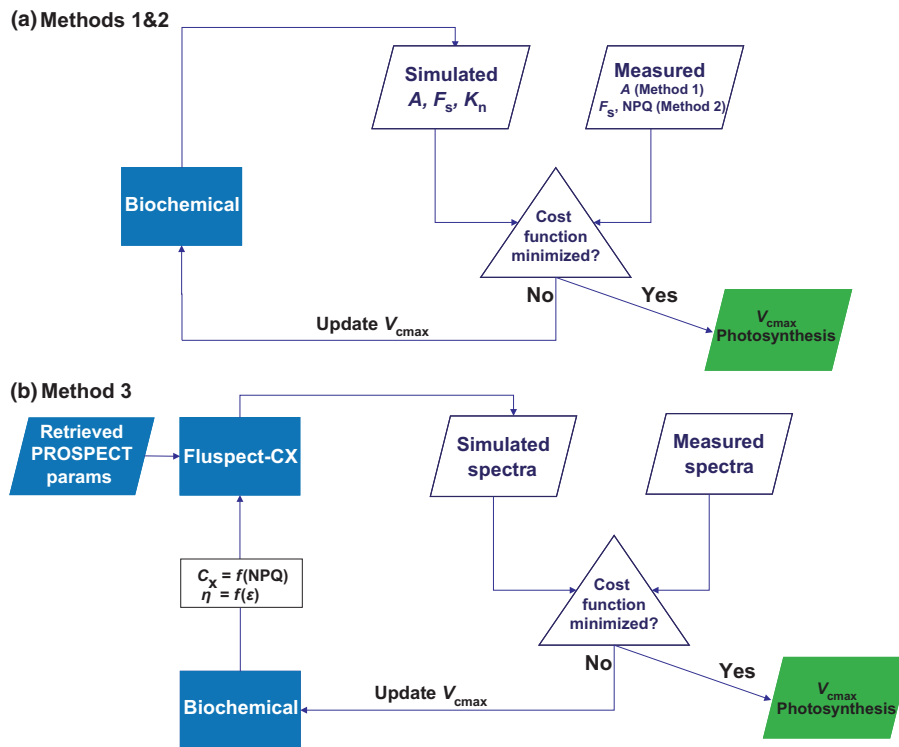
Fig. 2 The schematics for three methods of V_{cmax} retrieval. (a) In methods 1 and 2, the biochemical model is inverted by constraining the inversion with either the assimilation rate A curves (method 1) or with nonphotochemical quenching (NPQ) and steady-state fluorescence F_s curves (method 2). (b) In method 3, the combined model is inverted. First, the PROSPECT parameters (see Table 1) are retrieved once per leaf. Next, the biochemical model is initialized with standard input values. Parameters for photochemical reflectance C_x and fluorescence quantum efficiency η are prescribed as functions of NPQ and fluorescence emission efficiency ε, following Eqns 9 and 10, respectively. C_x and η, together with the estimated PROSPECT parameters, are provided as inputs of FLUSPECT. The difference between the FLUSPECT simulation and measured spectra is minimized by a cost function, resulting in the optimization of the chosen parameters.

Table 2 List of retrieved parameters, their initial values, lower boundaries (LB), upper boundaries (UB) and constraints per each investigated method.

Method	Retrieved parameter	Unit	Initial value	LB	UB	Constraint
1	V_{cmax}	$\mu mol\ CO_2\ m^{-2}\ s^{-1}$	70	0	250	Assimilation rate curves
2	V_{cmax}	$\mu mol\ CO_2\ m^{-2}\ s^{-1}$	70	0	250	
	K_n^0	—	2.48	2	6	F_s and NPQ curves
	β	—	0.114	0	100	
	γ	—	2.83	0	100	
3	V_{cmax}	$\mu mol\ CO_2\ m^{-2}\ s^{-1}$	70	0	250	ChlF and R or T spectra
	K_n^0	—	2.48	2	6	
	ς	—	0.007	0	0.2	

ChlF, Chl fluorescence; F_s, steady state fluorescence; R, reflectance; T, transmittance; NPQ, nonphotochemical quenching. For a full description of parameters, see Table 1.

same optical response. For the light curves, dynamics of both ΔPRI and (F_{740} are directly driven by the increasing light intensity. Their relations with A, Φ_{PSII}, NPQ and LUE above the peak value are almost linear, as well as their relations among each other. By contrast, the CO_2 curves produce a seemingly less predictable response, with higher variations in measured data, and less obvious relations between the spectral and other variables.

Differences between the two species are generally small (Figs 3, 4): sugar beet (*Beta vulgaris*) seems to have better capacity for using elevated CO_2 concentrations above 400 ppm, but light responses of the two species were similar. The difference between

control and reduced soil moisture content was small; for this reason we do not differentiate between species and treatments in the following results of V_{cmax} retrieval.

Retrievals of V_{cmax}

V_{cmax} and assimilation values estimated with the three methods are presented in Fig. 5, with supporting statistical information.

In Fig. 5(b) we compare V_{cmax} retrieved from CO_2- and light-response curves of the same leaves with method 1. The data display a high level of correlation ($R^2 = 0.82$ and RMSE ≈ 6), with

very accurate predictions of A (Fig. 5a; $R^2 = 0.98$ and RMSE ≈ 1).

The two other methods (Fig. 5e,h) capture the span of V_{cmax} for both types of response curves, with accurate predictions of A (Fig. 5d,g, with $R^2 > 0.80$ and RMSE < 4.6). Retrievals of V_{cmax} from PAM measurements provide the highest error (RMSE ≈ 20–23 µmol m^{-2} s^{-1}). Where hyperspectral data are used to constrain the model (Fig. 5h), for both CO_2 and light spectral responses, only the magnitude of V_{cmax} can be estimated (RMSE < 10), not the variation among leaves. Predictions of A are accurate, with $R^2 > 0.85$ and RMSE < 4.6.

The residuals (retrieved values minus the values retrieved from light curves with method 1) for the three methods are also shown (Fig. 5c,f,i). The smallest range of differences occurs with method 1, with unreliable estimations from method 2. Methods 2 and 3 show a consistent overestimation of V_{cmax}, especially at high V_{cmax} values.

Retrievals from the light-response curve have a better goodness-of-fit ($R^2 = 0.45$) than retrievals from CO_2-response curves ($R^2 = 0.081$). We evaluated other state variables besides V_{cmax} and A; Fig. 6 shows that whereas ETR, Φ_{PSII}, and K_n are estimated rather well, simulated F_s is poorly correlated to PAM-measured F_s. This holds for both the CO_2- and light-response curves, although the latter have a better goodness-of-fit.

The accuracy of spectral fit after optimization between measured and simulated τ or ChlF is presented in Fig. 7. The spectral fit of τ and forward ChlF at the selected wavelengths is similarly good, with error close to 0% on average, with a maximal deviation of 4% for τ and 17% for ChlF. The measurement error of the spectra used for V_{cmax} retrieval had a negligible effect on the estimated V_{cmax} (3%, not shown). Most of the uncertainty in V_{cmax} is due to the sensitivity of V_{cmax} to the spectra and the model representation. This is illustrated in Fig. 8, showing the RMSE used as the cost functions for the first and third methods as a function of V_{cmax} for one representative leaf. Both the RMSE of fluorescence and transmittance have a single minimum, indicating their sensitivity to V_{cmax}. The RMSE of fluorescence has a sharp and deep minimum, which confirms the sensitivity of fluorescence to V_{cmax}, but the location of the minimum differs between the CO_2- and light-response curves, which is indicative of a model representation error. The RMSE of transmittance shows a less sharp minimum, but the location of the minimum agrees between the CO_2 and light curves, and with the value retrieved from the
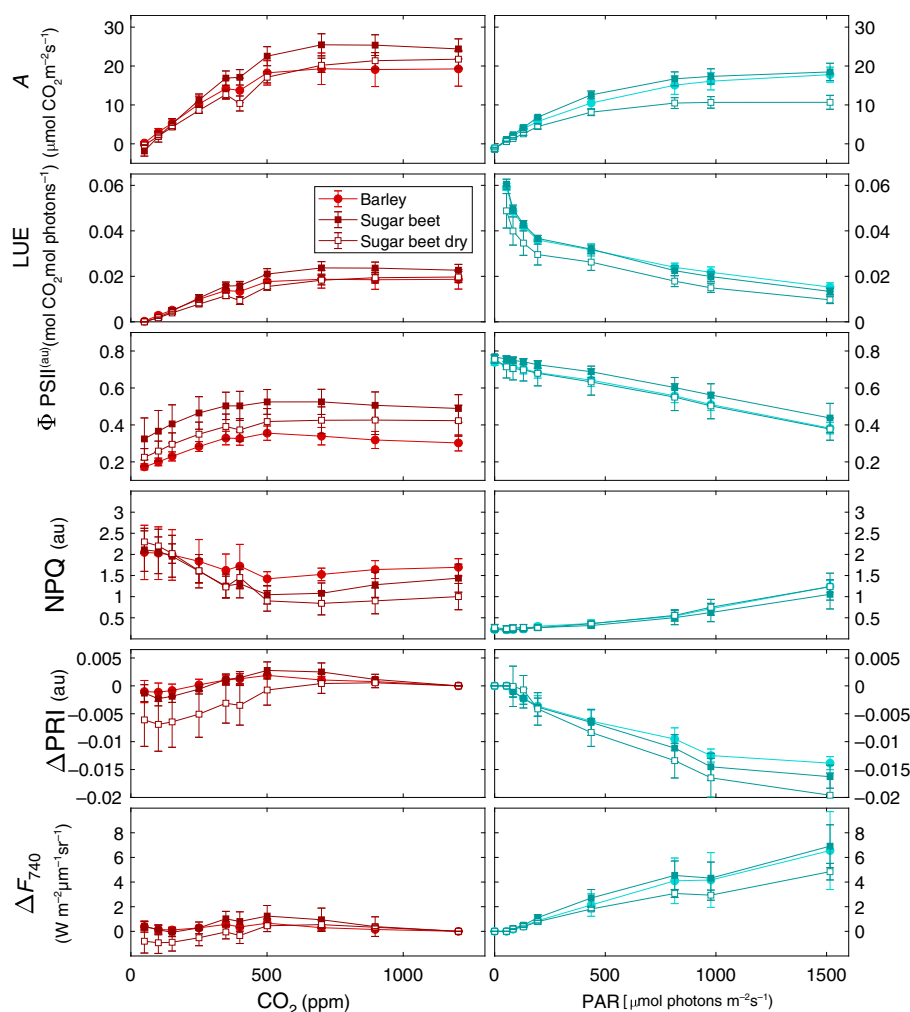

Fig. 3 Response to changing CO_2 concentrations and light intensity (photosynthetically active radiation, PAR) in barley (circles) and sugar beet (squares) leaves for (top to bottom): photosynthetic CO_2 assimilation (A); light use efficiency (LUE) of CO_2 assimilation; quantum efficiency of photosystem II (Φ_{PSII}); nonphotochemical quenching (NPQ); photochemical reflectance index (PRI) normalized to the most nonstressed state (ΔPRI); and Chl fluorescence at 740 nm normalized to the most nonstressed state (ΔF_{740}). The error bars represent $\pm$ SD from the mean. $n_{CO_2} = 20$ and $n_{light} = 17$.
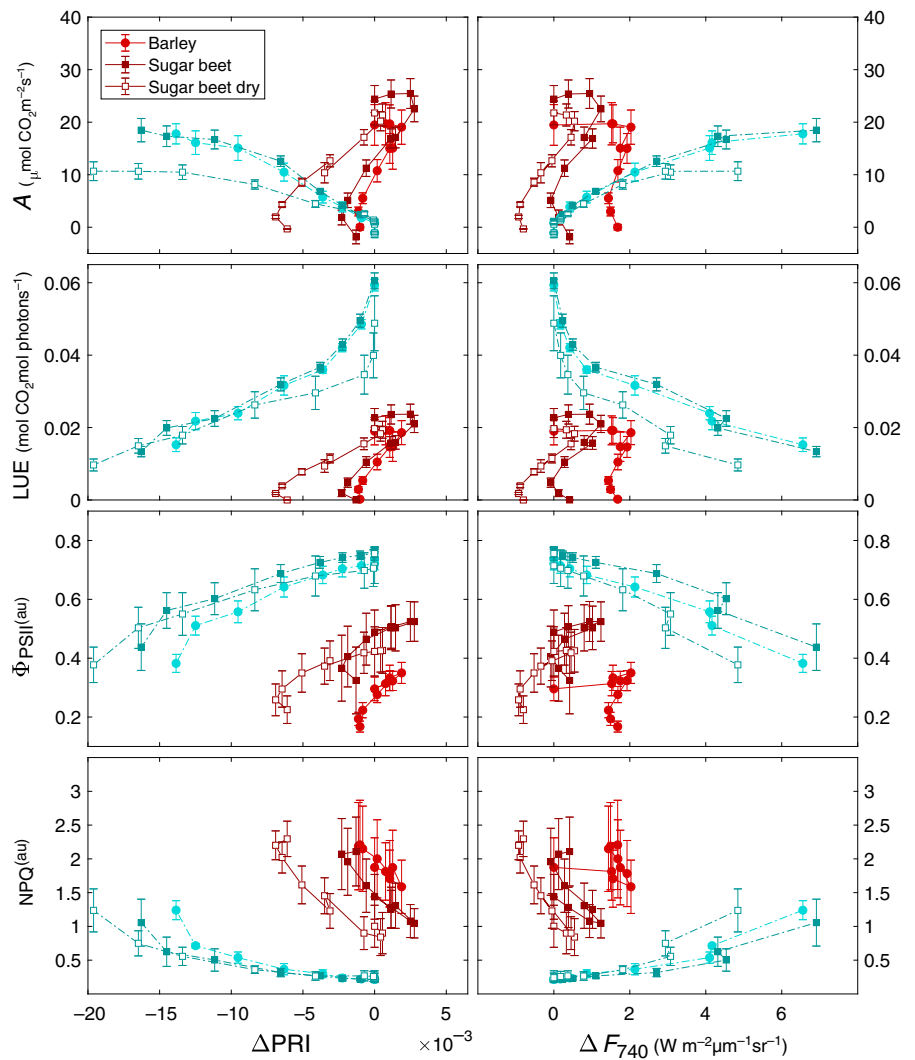
Fig. 4 Relation of photosynthetic CO_2 assimilation A; light use efficiency (LUE) of CO_2 assimilation; quantum efficiency of photosystem II (Φ_{PSII}) and nonphotochemical quenching (NPQ) to photochemical reflectance index (PRI) normalized to the most nonstressed state (ΔPRI); and Chl fluorescence at 740 nm normalized to the most nonstressed state (ΔF_{740}) under changing CO_2 concentrations (red, solid line) and light intensity (photosynthetically active radiation; blue, dotted line) in barley (circles) and sugar beet (squares) leaves. The error bars represent $\pm$ SD from the mean. $n_{CO_2} = 20$ and $n_{light} = 17$.

assimilation data with method 1. This indicates that the model cannot fully reproduce the measured spectrum, but the transmittance nevertheless responds to V_{cmax} and the model is able to identify the correct value of V_{cmax}.

We further investigate the separate contributions of the fitting parameters used in method 3 (V_{cmax}, K_n^0 and ς) to the spectra simulated by the combined model in Fig. 9. τ is influenced most by V_{cmax}, less by K_n^0, and -obviously- ς (the scaling of ChlF) has no effect on τ while ChlF is influenced mostly by ς, less by K_n^0, and the effect of V_{cmax} is still relatively small despite the clear sensitivity shown in Fig. 8.

Retrieving V_{cmax} from FluoWat data For the FluoWat data (Fig. 10), we obtained similar results as for the chamber dataset: the correct range of V_{cmax} values is retrieved (RMSE c. 13 µmol m^{-2} s^{-1}), but with low goodness-of-fit. The residuals have the same span as obtained for the chamber dataset (Fig. 5h), albeit reversed: there is an increase in underestimation with increasing V_{cmax} values. There are no substantial differences in results when transmittance or reflectance of the

leaf are used for the retrieval. It should be emphasized that we used the V_{cmax} values obtained earlier in the chamber for validation, because the FluoWat leaf clip does not allow for gas-exchange measurements.

Discussion

Both the transmittance and the fluorescence spectra (method 3) contain sufficient information to constrain V_{cmax}, as demonstrated by the clear minima in their RMSE with respect to varying V_{cmax} (Fig. 8). The results show that, for our dataset, with limiting span of V_{cmax}, the magnitude but not the variability of V_{cmax} among leaves can be estimated from the coupled model, by using the combined information of hyperspectral ChlF and green ρ or τ. The RMSE for the estimated V_{cmax} is nevertheless below 14 µmol CO_2 m^{-2} s^{-1}, which complies with the error determined by similar studies of leaf level responses (Serbin *et al.*, 2012; Dechant *et al.*, 2017) and by a study on airborne data by Serbin *et al.* (2015). Both Serbin *et al.* (2012) and Dechant *et al.* (2017) used a much

wider range of V_{cmax} (0–200 µmol CO_2 m^{-2} s^{-1}). Considering the limited span of V_{cmax} in our measurements (50–100 µmol CO_2 m^{-2} s^{-1}), the low and comparable values of

RMSE are encouraging. Leaf datasets with a known wider span of maximum photosynthetic capacity would provide a valuable further validation of the model.
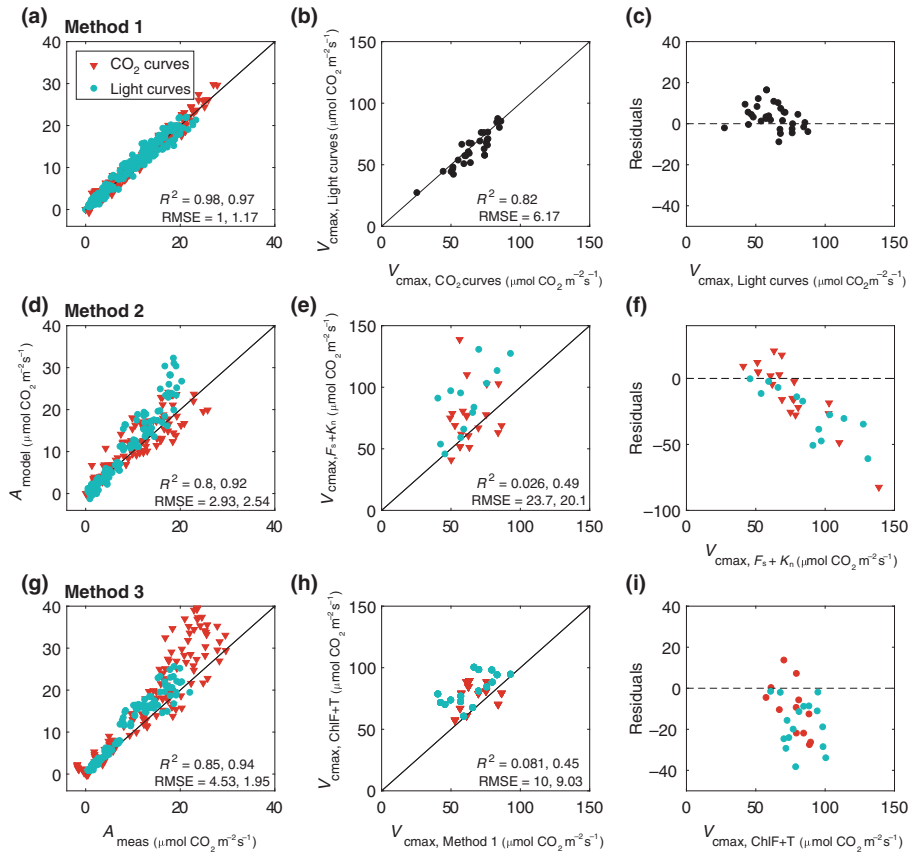

Fig. 5 Maximum carboxylation capacity V_{cmax} and assimilation rate A, estimated with three different methods (a,b,d,e,g,h), together with residuals of predictions (measured minus estimated V_{cmax}, c,f,i). In method 1 (a–c), we compare V_{cmax} retrieved from CO_2-response curves with the ones retrieved from light-response curves. In methods 2 (d–f) and 3 (g–i) we compare the V_{cmax} retrieved from either pulse amplitude modulation measurements of steady-state fluorescence F_s and nonphotochemical quenching K_n or hyperspectral measurements of Chl fluorescence and transmittance τ, respectively, with the values estimated with method 1. Number of samples (leaves) for CO_2- and light-response curves per method is $n_{m1} = 34/34$, $n_{m2} = 19/13$, and $n_{m3} = 12/16$. Pearson's correlation coefficient R^2 and RMSE are shown per measurements type, CO_2 (red triangles) and light curves (blue circles).
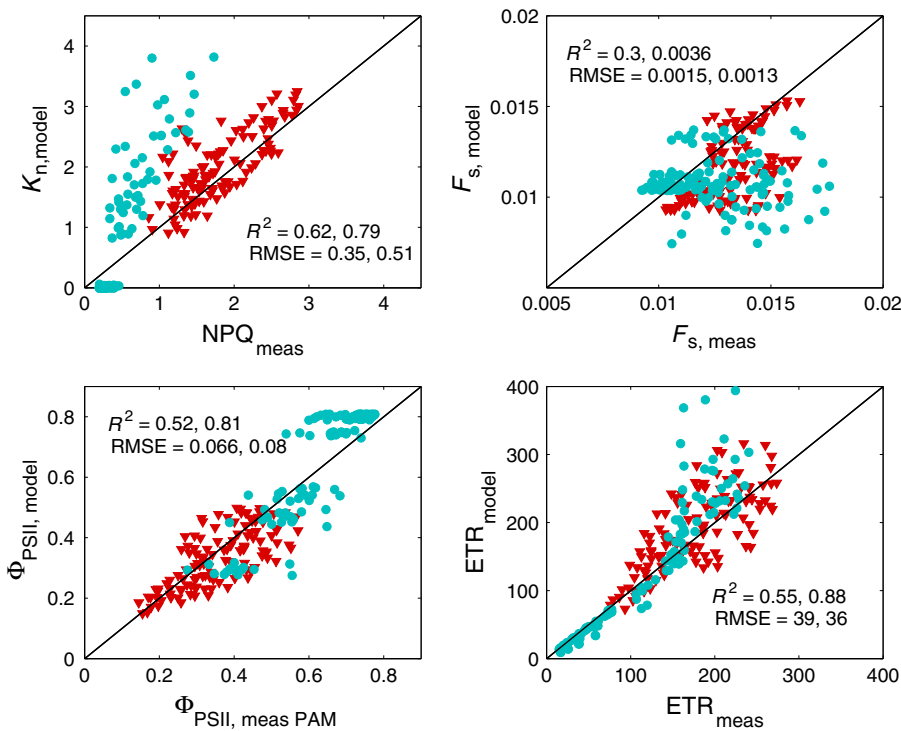

Fig. 6 Modelled vs measured nonphotochemical quenching (K_n or NPQ), steady-state fluorescence F_s, quantum efficiency of photosystem II (Φ_{PSII}), and electron transport rate (ETR) for method 3. Pearson's correlation coefficient R^2 and RMSE are shown per measurements type, CO_2 (red triangles) and light curves (blue circles). $n_{CO_2} = 12$ and $n_{light} = 16$.

The response of ChlF to changing CO_2 is small, but neverthe-less meaningful (see dashed line in Fig. 8c). This response is limited due to the fact that in a CO_2-response curve, a reduction of PQ is compensated by an increase in NPQ and vice versa, with limited net effect on ChlF. The responses of NPQ and ΔPRI are unambiguous, but tuning V_{cmax} cannot bring the RMSE of transmittance close to zero (Fig. 8b): the effect of NPQ on transmittance is small compared with the accuracy by which we can reproduce the overall transmittance spectrum.

Potential errors in the V_{cmax} retrieval with method 3 include measurement errors, the performance of the optimization method, and the biochemical and radiative transfer model representation. We investigated the potential effects of measurement errors and accuracy of spectral fit on the retrievals of V_{cmax}, but

these effects were minimal: up to 3% of the retrieved V_{cmax} values. Crucial is the model representation.

Despite controlled experimental conditions, the values of V_{cmax} estimated from the assimilation rates (method 1) differ up to 25% between light and CO_2 responses (Fig. 5c). A study by Miao *et al.* (2009) has similarly shown that significant differences exist between different methods of V_{cmax} retrieval from *A* curves. This could be attributed to limitations of the Collatz model (Collatz *et al.*, 1991) used by Van der Tol *et al.* (2014), which does not use the maximum electron transport capacity J_{max} of the original Farquhar model as an additional parameter. The parameterization of photorespiration may also contribute to this difference; photorespiration was not suppressed in our experiment, which was carried out under ambient O_2.
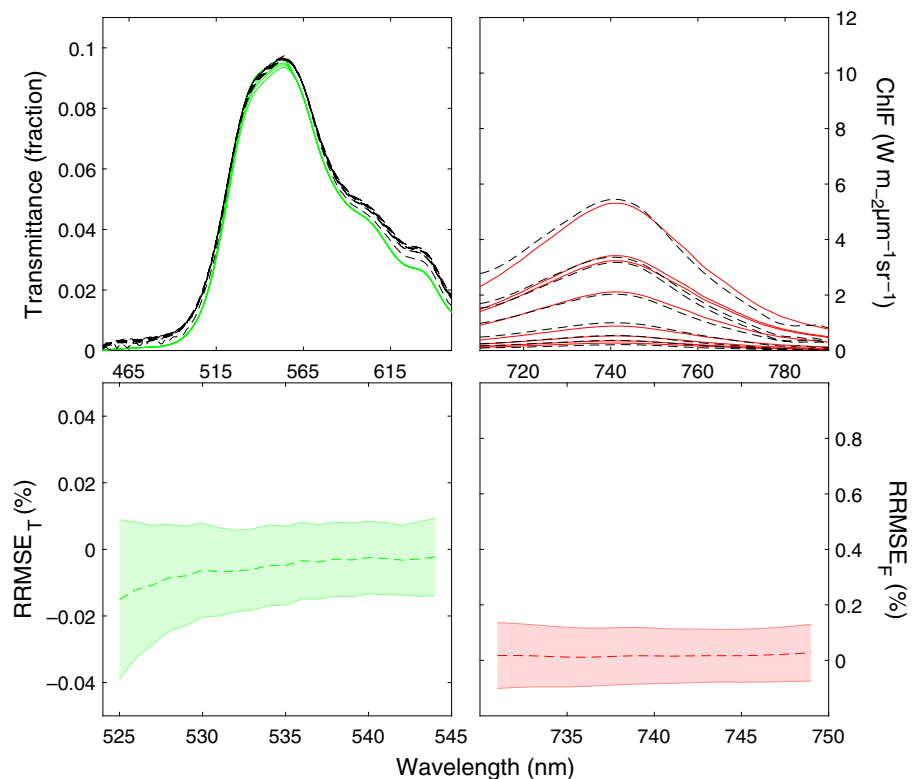

Fig. 7 Comparison of measurements (broken line, black) and retrieval accuracy (solid line, red) after fitting with method 3 in the selected bands of transmittance (left panels) and forward Chl fluorescence (ChlF, right panels) spectra. RRMSE is the relative root-mean-square error of retrieval accuracy, and the shaded area represents the SD of the mean (broken line).
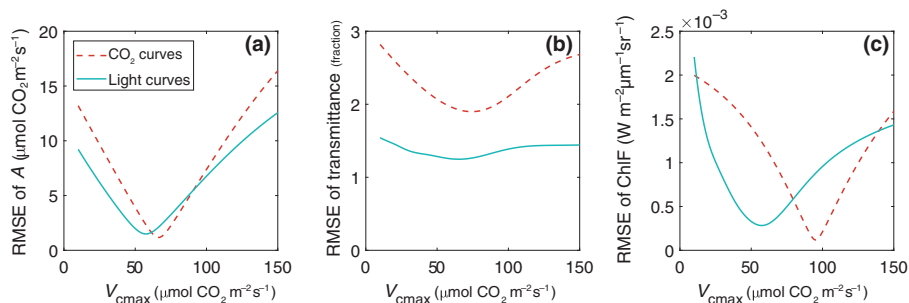

Fig. 8 RMSE used as the cost functions for methods 1 and 3 as a function of maximum carboxylation capacity V_{cmax} for one representative leaf, plotted as the input range of V_{cmax} against the corresponding RMSE of (a) either assimilation rate (method 1) or (b) transmittance (method 3) and (c) fluorescence (method 3). The valleys of the curves represent the minima of the V_{cmax} optimization.

Differences in the optimized values from transmittance and fluorescence (Fig. 8b,c) may originate from the prescribed relations of η and C_x to ε and K_n, which were reconciled by using a single cost function for both transmittance and fluorescence, and allowing variations in these relationships.

We established the link between the radiative transfer model FLUSPECT and the photosynthesis model via parameter η (the absolute ChlF quantum yield) to $\varepsilon = F_s/F_o$, and C_x to K_n via a calibrated coefficient (Vilfan *et al.*, 2018). This introduces uncertainty, because PAM F_s cannot be reproduced well by the model. The poor correlation of PAM F_s to simulated F_s can at least
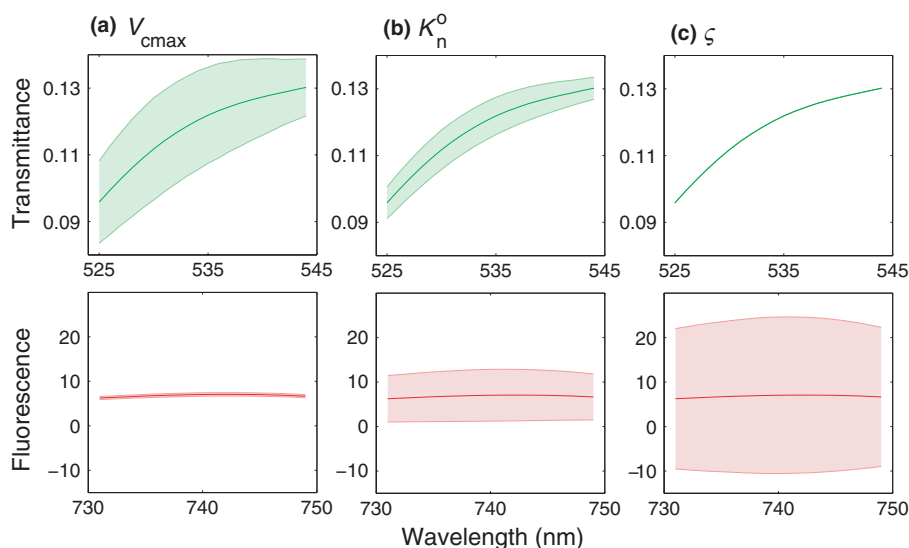
Fig. 9 Sensitivity of transmittance (upper panels) and Chl fluorescence (ChlF, lower panels) spectra to the three fitting parameters used in method 3: (a) maximum carboxylation capacity V_{cmax}; (b) K_n^0 (fitting parameter for nonphotochemical quenching K_n; Eqn 4); and (c) the scaling factor ς that links the ChlF efficiencies of the two leaf models in Eqn 10. The shaded area denotes the span of values.
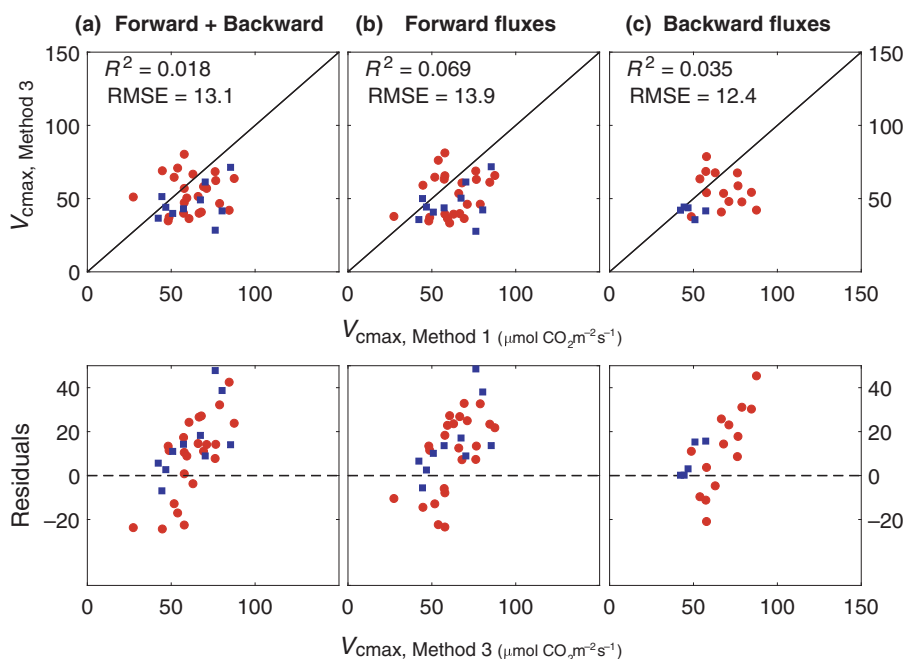

Fig. 10 Values of maximum carboxylation capacity V_{cmax}, retrieved for the FluoWat dataset with method 3, vs control values for barley (red circles) and sugar beet (blue squares) leaves, with the residuals (measured minus estimated V_{cmax}) shown in the bottom panels. V_{cmax}, K_n^0 (fitting parameter for K_n; Eqn 4), and the scaling factor ς (links the Chl fluorescence (ChlF) efficiencies of the two leaf models in Eqn 10) were optimized to best reproduce measured (a) reflectance and backward ChlF, (b) transmittance and forward ChlF, or (c) all four simultaneously. Pearson's correlation coefficient (R^2) and RMSE are shown for all data combined. Note, that the control values of V_{cmax} ($V_{cmax,\text{Method 1}}$) were obtained by applying method 1 to the Chamber dataset. Number of samples for barley and sugar beet per retrieval is $n_a = 23/10$, $n_b = 23/10$, and $n_c = 14/5$.

partly be explained by the compensation of the effects of PQ and NPQ, resulting in a relatively small range of F_s, which is then prone to uncertainties. This was also noted in the development of the extended biochemical model (Van der Tol *et al.*, 2014, Fig. 9).

In Van der Tol *et al.* (2014), two different parametrizations are given for K_n for different datasets. Obviously, K_n^0, a parameter for the xanthophyll pool size, may vary. In a first attempt to fit τ and ChlF of the light-response curves, we found that retrieving only V_{cmax} while keeping K_n^0 at the default value of Van der Tol *et al.* (2014) did not provide a satisfactory fit (not shown here). It was necessary, therefore, to include K_n^0 in the retrieval. Inclusion of ς was necessary in order to translate F_s in arbitrary units to absolute values of ChlF yield.

Indeed, the sensitivity analysis (Figs 8, 9) reveals that τ simulated with the combined model depends primarily on V_{cmax}, whereas the magnitude of ChlF is most affected by the hitherto unconstrained ς, and K_n^0 has a similar effect on both indicators. These results indicate that both τ and ChlF contribute to the V_{cmax} estimations.

Potential ill-posedness could be reduced by introducing prior information on V_{cmax}; for example, based on vegetation indices or pigment concentrations, of which Chl concentration is a most valid candidate (Houborg *et al.*, 2015; Gitelson *et al.*, 2016). A more mechanistic modelling could potentially reduce the uncertainty in other parameters, such as K_n^0 and ς. For example, the description of energy partitioning to NPQ used in this study could be replaced with MD12, whereas models developed by Zaks *et al.* (2013) and Matuszyńska *et al.* (2016) may help constrain ς using fluorescence kinetics.

The residuals of two datasets (chamber vs leaf clip) used with method 3 (Figs 5i, 9) have the same span, which is encouraging, as it shows that similar results can be achieved with different types of spectral measurements (i.e. reflectance or transmittance). In general, predictions of A are at least 10% more accurate for estimations from light-response curves compared with CO_2 responses; and similarly, light-response curves provide a higher accuracy of V_{cmax} retrieval.

Our study showed that a quantification of photosynthesis from transmittance or reflectance and ChlF during light- and CO_2-response curves is possible and very promising.

Acknowledgements

Author contributions

NV is the main author of this paper; she collected the datasets, coupled the models, and performed the analysis. CvdT and WV assisted with model development, sensitivity analysis, and manuscript development.

ORCID

Christiaan van der Tol (iD) https://orcid.org/0000-0002-2484-8191
Wouter Verhoef (iD) https://orcid.org/0000-0003-4696-2144
Nastassia Vilfan (iD) https://orcid.org/0000-0002-4834-1918

References

Ač A, Malenovský Z, Olejníčková J, Gallé A, Rascher U, Mohammed G. 2015. Meta-analysis assessing potential of steady-state chlorophyll fluorescence for remote sensing detection of plant water, temperature and nitrogen stress. *Remote Sensing of Environment* **168**: 420–436.

Atherton J, Nichol CJ, Porcar-Castell A. 2016. Using spectral chlorophyll fluorescence and the photochemical reflectance index to predict physiological dynamics. *Remote Sensing of Environment* **176**: 17–30.

Barton CVM, North PRJ. 2001. Remote sensing of canopy light use efficiency using the photochemical reflectance index: model and sensitivity analysis. *Remote Sensing of Environment* **78**: 264–273.

Björkman O. 1981. Responses to different quantum flux densities. In: Lange OL, Nobel PS, Osmond CB, Ziegler H, eds. *Physiological plant ecology I.* Berlin, Germany: Springer, 57–107.

Cheng YB, Middleton EM, Zhang Q, Huemmrich KF, Campbell PKE, Corp LA, Cook BD, Kustas WP, Daughtry CS. 2013. Integrating solar induced fluorescence and the photochemical reflectance index for estimating gross primary production in a cornfield. *Remote Sensing* **5**: 6857–6879.

Collatz GJ, Ball JT, Grivet C, Berry JA. 1991. Physiological and environmental regulation of stomatal conductance, photosynthesis and transpiration: a model that includes a laminar boundary layer. *Agricultural and Forest Meteorology* **54**: 107–136.

Dechant B, Cuntz M, Vohland M, Schulz E, Doktor D. 2017. Estimation of photosynthesis traits from leaf reflectance spectra: correlation to nitrogen content as the dominant mechanism. *Remote Sensing of Environment* **196**: 279–292.

Demmig-Adams B, Adams WW III. 1996. The role of xanthophyll cycle carotenoids in the protection of photosynthesis. *Trends in Plant Science* **1**: 21–26.

Drusch M, Moreno J, Del Bello U, Franco R, Goulas Y, Huth A, Kraft S, Middleton EM, Miglietta F, Mohammed G et al. 2017. The FLuorescence EXplorer mission concept — ESA's Earth Explorer 8. *IEEE Transactions on Geoscience and Remote Sensing* **55**: 1273–1284.

Farquhar GD, von Caemmerer S, Berry JA. 1980. A biochemical model of photosynthetic CO_2 assimilation in leaves of C_3 species. *Planta* **149**: 78–90.

Féret J-B, Gitelson AA, Noble SD, Jacquemoud S. 2017. PROSPECT-D: towards modeling leaf optical properties through a complete lifecycle. *Remote Sensing of Environment* **193**: 204–215.

Franck F, Juneau P, Popovic R. 2002. Resolution of the photosystem I and photosystem II contributions to chlorophyll fluorescence of intact leaves at

New
Phytologist

room temperature. *Biochimica et Biophysica Acta (BBA) – Bioenergetics* **1556**: 239–246.

Gamon JA, Peñuelas J, Field CB. 1992. A narrow-waveband spectral index that tracks diurnal changes in photosynthetic efficiency. *Remote Sensing of Environment* **41**: 35–44.

Garbulsky MF, Peñuelas J, Gamon J, Inoue Y, Filella I. 2011. The photochemical reflectance index (PRI) and the remote sensing of leaf, canopy and ecosystem radiation use efficiencies. A review and meta-analysis. *Remote Sensing of Environment* **115**: 281–297.

Gitelson AA, Gamon JA, Solovchenko A. 2017. Multiple drivers of seasonal change in PRI: implications for photosynthesis 1. Leaf level. *Remote Sensing of Environment* **191**: 110–116.

Gitelson AA, Peng Y, Arkebauer TJ, Suyker AE. 2015. Productivity, absorbed photosynthetically active radiation, and light use efficiency in crops: implications for remote sensing of crop primary production. *Journal of Plant Physiology* **177**: 100–109.

Gitelson AA, Peng Y, Viña A, Arkebauer T, Schepers JS. 2016. Efficiency of chlorophyll in gross primary productivity: a proof of concept and application in crops. *Journal of Plant Physiology* **201**: 101–110.

Grace J, Nichol C, Disney M, Lewis P, Quaife T, Bowyer P. 2007. Can we measure terrestrial photosynthesis from space directly, using spectral reflectance and fluorescence? *Global Change Biology* **13**: 1484–1497.

Houborg R, McCabe MF, Cescatti A, Gitelson AA. 2015. Leaf chlorophyll constraint on model simulated gross primary productivity in agricultural systems. *International Journal of Applied Earth Observation and Geoinformation* **43**: 160–176.

Jacquemoud S, Baret F. 1990. PROSPECT: a model of leaf optical properties spectra. *Remote Sensing of Environment* **34**: 75–91.

Kosugi Y, Matsuo N. 2006. Seasonal fluctuations and temperature dependence of leaf gas exchange parameters of co-occurring evergreen and deciduous trees in a temperate broad-leaved forest. *Tree Physiology* **26**: 1173–1184.

Liu L, Guan L, Liu X. 2017. Directly estimating diurnal changes in GPP for C$_3$ and C$_4$ crops using far-red sun-induced chlorophyll fluorescence. *Agricultural and Forest Meteorology* **232**: 1–9.

Matuszyńska A, Heidari S, Jahns P, Ebenhöh O. 2016. A mathematical model of non-photochemical quenching to study short-term light memory in plants. *Biochimica et Biophysica Acta – Bioenergetics* **1857**: 1860–1869.

Maxwell K, Johnson GN. 2000. Chlorophyll fluorescence—a practical guide. *Journal of Experimental Botany* **51**: 659–668.

Miao Z, Xu M, Lathrop RG, Wang Y. 2009. Comparison of the $A–C_c$ curve fitting methods in determining maximum ribulose 1,5-bisphosphate carboxylase/oxygenase carboxylation rate, potential light saturated electron transport rate and leaf dark respiration. *Plant, Cell & Environment* **32**: 109–122.

Peñuelas J, Filella I, Gamon JA. 1995. Assessment of photosynthetic radiation-use efficiency with spectral reflectance. *New Phytologist* **131**: 291–296.

Ruban AV. 2016. Nonphotochemical chlorophyll fluorescence quenching: mechanism and effectiveness in protecting plants from photodamage. *Plant Physiology* **170**: 1903–1916.

Serbin SP, Dillaway DN, Kruger EL, Townsend PA. 2012. Leaf optical properties reflect variation in photosynthetic metabolism and its sensitivity to temperature. *Journal of Experimental Botany* **63**: 489–502.

Serbin SP, Singh A, Desai AR, Dubois SG, Jablonski AD, Kingdon CC, Kruger EL, Townsend PA. 2015. Remotely estimating photosynthetic capacity, and its response to temperature, in vegetation canopies using imaging spectroscopy. *Remote Sensing of Environment* **167**: 78–87.

Tremblay N, Wang Z, Cerovic ZG. 2011. Sensing crop nitrogen status with fluorescence indicators. A review. *Agronomy for Sustainable Development* **32**: 451–464.

Van der Tol C, Berry JA, Campbell PKE, Rascher U. 2014. Models of fluorescence and photosynthesis for interpreting measurements of solar-induced chlorophyll fluorescence. *Journal of Geophysical Research. G, Biogeosciences* **119**: 2312–2327.

Van der Tol C, Verhoef W, Timmermans J, Verhoef A, Su Z. 2009. An integrated model of soil-canopy spectral radiances, photosynthesis, fluorescence, temperature and energy balance. *Biogeosciences* **6**: 3109–3129.

Van Wittenberghe S, Alonso L, Verrelst J, Hermans I, Delegido J, Veroustraete F, Valcke R, Moreno J, Samson R. 2013. Upward and downward solar-induced chlorophyll fluorescence yield indices of four tree species as indicators of traffic pollution in Valencia. *Environmental Pollution* **173**: 29–37.

Vilfan N, Van der Tol C, Muller O, Rascher U, Verhoef W. 2016. FLUSPECT-B: a model for leaf fluorescence, reflectance and transmittance spectra. *Remote Sensing of Environment* **186**: 596–615.

Vilfan N, Van der Tol C, Yang P, Wyber R, Malenovský Z, Robinson SA, Verhoef W. 2018. Extending FLUSPECT to simulate xanthophyll driven leaf reflectance dynamics. *Remote Sensing of Environment* **211**: 345–356.

Walker AP, Beckerman AP, Gu L, Kattge J, Cernusak LA, Domingues TF, Scales JC, Wohlfahrt G, Wullschleger SD, Woodward FI. 2014. The relationship of leaf photosynthetic traits – V_{cmax} and J_{max} – to leaf nitrogen, leaf phosphorus, and specific leaf area: a meta-analysis and modeling study. *Ecology and Evolution* **4**: 3218–3235.

Wieneke S, Ahrends H, Damm A, Pinto F, Stadler A, Rossini M, Rascher U. 2016. Airborne based spectroscopy of red and far-red sun-induced chlorophyll fluorescence: implications for improved estimates of gross primary productivity. *Remote Sensing of Environment* **184**: 654–667.

Zaks J, Amarnath K, Sylak-Glassman EJ, Fleming GR. 2013. Models and measurements of energy-dependent quenching. *Photosynthesis Research* **116**: 389–409.

Zhang Y, Guanter L, Berry JA, Van der Tol C, Yang X, Tang J, Zhang F. 2016. Model-based analysis of the relationship between sun-induced chlorophyll fluorescence and gross primary production for remote sensing applications. *Remote Sensing of Environment* **187**: 145–155.

Zheng T, Chen J, He L, Arain MA, Thomas SC, Murphy JG, Geddes JA, Black TA. 2017. Inverting the maximum carboxylation rate (V_{cmax}) from the sunlit leaf photosynthesis rate derived from measured light response curves at tower flux sites. *Agricultural and Forest Meteorology* **236**: 48–66.